A Dual-ISM-Band Antenna of Small Size Using a Spiral Structure with Parasitic Element

J. L. Buckley, *Member, IEEE,* K. G. McCarthy, *Member, IEEE,* L. Loizou, *Member, IEEE,* B. O' Flynn, *Member, IEEE, C.* O' Mathuna, *Fellow, IEEE*

***Abstract*— This letter presents a compact, single-feed, dual-band antenna covering both the 433 MHz and 2.45 GHz Industrial Scientific and Medical (ISM) bands. The antenna has small dimensions of 51 × 28 mm^2. A square-spiral resonant element is printed on the top layer for the 433 MHz band. The remaining space within the spiral is used to introduce an additional parasitic monopole element on the bottom layer that is resonant at 2.45 GHz. Measured results show that the antenna has a -10 dB bandwidth of 2 MHz at 433 MHz and 132 MHz at 2.45 GHz respectively. The antenna has omni-directional radiation characteristics with a peak realized gain (measured) of -11.5 dBi at 433 MHz and +0.5 dBi at 2.45 GHz respectively.**

***Index Terms*—Antenna, Compact, Dual-Band, IFA, QoS.**

I. INTRODUCTION

WIRELESS sensor network (WSN) technology is rapidly emerging in application areas such as smart healthcare and fitness monitoring. These systems are typically small, battery powered devices operating in the 2.45 GHz ISM band using the IEEE 802.15.4 standard. However, the availability of other license-free bands such as the 433 MHz ISM band in Europe provides potential for Quality of Service (QoS) improvements. For example, the ability to adaptively switch from the 2.45 GHz to the 433 MHz ISM band can provide potential such as reduced signal attenuation in biological monitoring applications as well as improved immunity to interference and congestion. Band switching can also offer improvements in data reliability, availability and security when compared with existing solutions [1].

The requirement to switch between frequency bands poses a number of design challenges however, because small, low-cost antenna structures with multi-band capability are necessary. This area has been the subject of intense research in recent years with a large number of multi-band antennas reported in the literature. These include a dual-band, inverted-F antenna (IFA) for 433/868 MHz [2], a printed-loop for 900/1800 MHz cellular applications [3] and a triple-band inverted-L topology for 2.4/5.2/5.8 GHz WLAN applications [4]. Other approaches use reconfigurable antennas where the antenna topology can be controlled electronically, for example using active RF switches [5]. Most passive, multi-band antennas are generally resonant at a fundamental and a harmonic, or near harmonic, of the fundamental frequency. Only a limited number of small sized, passive-type antennas are described in the literature that can cover both the lower and upper extents of the ISM bands, such as dual-band operation at 433 MHz and 2.45 GHz. Examples of small, multi-band topologies are described in [6, 7] but are designed for bio-implantable applications.

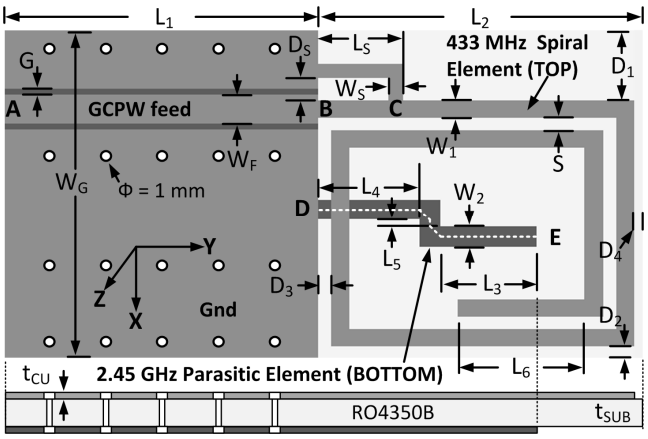

Fig. 1. Configuration of new dual-band 433 MHz / 2.45 GHz antenna.

A small-sized antenna design is reported in [8] using a capacitively loaded IFA topology and a parasitic element to achieve dual-band operation at 930 MHz and 1.7 GHz. A conventional IFA requires a minimum size of λ/4 but this antenna is realized in a size of 0.109λ × 0.025λ, not including a groundplane. The design of electrically small antennas is challenging however as significantly decreasing the antenna size can adversely affect bandwidth, efficiency and gain performance [9]. An electrically small antenna was recently reported by the authors covering the 433 MHz ISM band [10]. In this paper, we implement improvements to this antenna to allow coverage of the 2.45 GHz ISM band. The size of the original antenna is maintained at 0.07λ × 0.05λ (at 433 MHz) including the groundplane.

This letter is organized as follows. Section II presents the proposed antenna topology. Section III describes antenna simulation and parametric analysis. Section IV presents the experimental results and discussion and Section V concludes the paper.

Manuscript received Month, Day, 2015. This work was supported by the EC SMArt Systems Co-design project (SMAC) FP7-ICT-2011-7-288827.

J. L. Buckley and B. O'Flynn are with the Tyndall National Institute, Lee Maltings, Cork, Ireland (e-mail: john.buckley @ tyndall.ie; brendan.oflynn @ tyndall.ie).

K. G. McCarthy is with the School of Engineering, Electrical and Electronic Engineering, University College Cork, Cork, Ireland (e-mail: k.mccarthy @ ucc.ie).

L. Loizou was with the Tyndall National Institute and is now with Benetel Ltd., Guinness Enterprise Centre, Dublin 8, (e-mail: loizos.loizou@ieee.org).

C. Ó Mathúna is with the Tyndall National Institute and Dept of Electrical and Electronic Engineering, University College Cork, Cork, Ireland (e-mail: c.omatuna @ tyndall.ie).

II. ANTENNA TOPOLOGY

Fig. 1 shows the configuration of the proposed dual-band antenna. The antenna structure is printed on a 1 Oz, 1.524 mm, double-sided RO4350B laminate with a relative permittivity ε_R = 3.6 and loss tangent tanδ = 0.0031. The total size of the antenna is 51 mm × 27.4 mm and it is excited using a 50-Ω grounded-coplanar-waveguide (GCPW) feed-line at Point *A* shown that is referenced to ground on both the top and bottom layers. A ground plane is printed on the bottom side of the substrate with dimensions of $W_G \times L_1$ and the co-planar ground structures on the top side are connected to the ground plane using a series of through-hole vias as shown.

For the Lower Band (433 MHz), a square-spiral structure of width W_1 is printed on the top layer at the end of the feed line at Point *B*. This structure is a variation of an IFA topology with the spiral used to minimize the required area for this resonant section. At Point *C*, similar to an IFA configuration, a shunt inductive element is used to allow impedance matching of the antenna impedance to 50-Ω without the need for discrete matching components.

For the Upper Band (2.45 GHz), a parasitic monopole element is printed on the bottom layer at Point *D* with the element shorted to the groundplane as shown. This element has a width W_2 and a total length of $L_3 + L_4 + L_5 + \sqrt{2}\,W_2$ as defined along the centre of the element as shown. The monopole is staggered to maximize the monopole length and minimize the degree of end-coupling to the spiral at Point *E*.

III. ANTENNA SIMULATION

A. Antenna Resonant Behaviour

The generalized resonant behaviour of the antenna *with* and *without* the parasitic monopole element was first studied in simulation using a full-wave EM model of the antenna and solved using ANSYS HFSS [11]. Table 1 in Section III (B) lists the parameters that were employed, except for L_6, L_3 and L_S that are specified here as L_6 = 10 *mm*, L_3 = 5 *mm* and L_S = 5 *mm* and whose values were later optimized. Fig. 2 shows the simulated return loss from 300 MHz to 3 GHz. The multi-band response of the antenna relates fundamentally to the intrinsic resonant properties of the spiral element which was designed to have a total electrical length of ≈ λ/4 at f_0 =433 MHz. The simulated response in Fig. 2 shows that with only the spiral element present, three distinct resonances are observed. The lowest resonance is shown at f_0, with two, higher frequency resonances observed at approximately odd multiples of f_0 i.e. $3f_0$ and $5f_0$. This behaviour is characteristic of a λ/4 antenna structure that has harmonic resonances at odd multiples of the

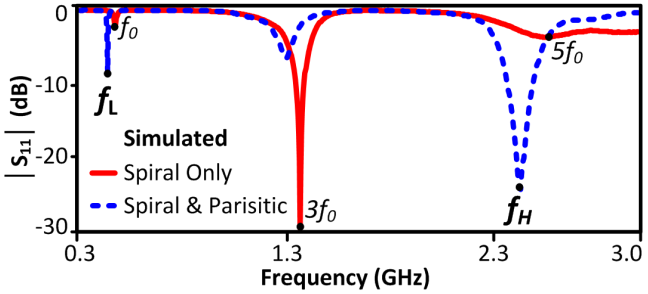

Fig. 2. Simulated return loss of antenna with and without parasitic element.

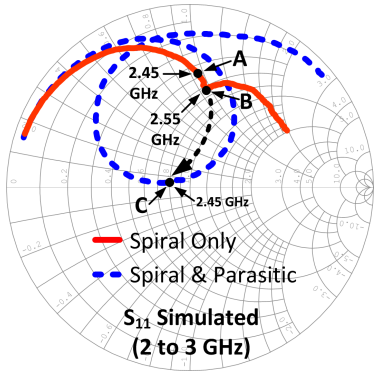

Fig. 3. Simulated S_{11} of the antenna with and without the parasitic element.

antenna's fundamental frequency [12]. The resonance at $3f_0$, or approximately 1.3 GHz, lies well outside both the ISM bands of interest and is therefore not considered further for this application. The resonances at f_0 and $5f_0$ are approximately 5% and 10% above the upper limits of the 433 MHz and 2.45 GHz ISM bands, respectively, but are not well matched to the 50-Ω source impedance. It can be seen from Fig. 2 that adding the parasitic element leads to a similar resonant response. However, in this case, with the monopole present, the three resonant frequencies occur at lower frequencies and the impedance matching is greatly improved at the two frequencies of interest for this application (f_L are f_H).

In order to better understand this behaviour, Fig. 3 plots the simulated antenna input impedance with and without the parasitic element present from 2 to 3 GHz. It can be seen that at Point *A*, with only the spiral element present, the antenna input impedance at 2.45 GHz is non-resonant or inductive. At Point *B*, a loop in the impedance profile is also observed at 2.55 GHz, corresponding to the return loss minimum at $5f_0$ in Fig. 2. When the parasitic monopole element is now introduced, a net capacitive loading effect is observed that results in a lowering of the resonant frequency from 2.55 to 2.45 GHz as well as enabling the antenna input impedance to be matched close to 50-Ω at 2.45 GHz (shown graphically as the movement from Point *B* to Point *C*). In order to visualize the resonant modes of the antenna, the simulated surface current distributions are plotted in vector form in Fig. 4. It can be seen from Fig. 4(a) that a large current flows on the spiral element at 433 MHz, with very little current flow on the parasitic monopole element. Fig. 4(b) shows that at 2.45 GHz, the spiral has a second resonant mode, with 3 current maxima and 2 current minima present, indicating that the spiral has an

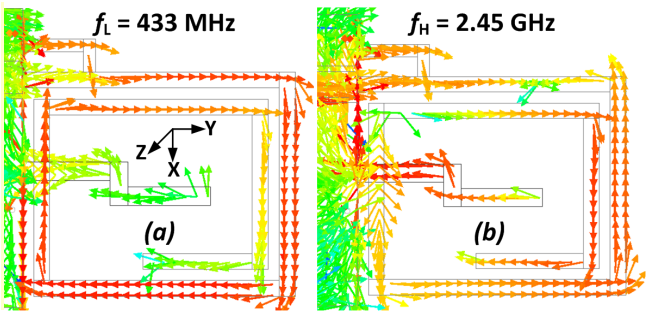

Fig. 4. Simulated antenna surface current distribution, (a) 433 MHz with J_{SURF_MAX} = 20 A/m, (b) 2.45 GHz with J_{SURF_MAX} = 5 A/m.

electrical length of ≈ 5λ/4 at 2.45 GHz. In this case, a large current flows on the parasitic element which has a resonant length of ≈ λ/4 at 2.45 GHz and is excited via mutual coupling with the driven spiral element. Fig. 4(b) also shows that in-phase currents occur mainly on the horizontal sections of the spiral element with out-of-phase currents observed largely on adjacent vertical sections. The combined radiation from the spiral and parasitic elements is therefore expected to be monopole-like, mainly due to the large currents flowing on the parasitic element at 2.45 GHz leading to enhanced radiation in the x-z plane with nulls present along the y-axis.

B. *Parametric Analysis*

In order to optimize the antenna for dual-band operation, the effects of several key parameters were investigated. Note that for subsequent discussion and presentation of results, only the Lower and Upper Band responses are considered and for clarity are plotted separately. The influence of the spiral length on the lower and upper bands was first studied. The spiral end-length L_6 was varied while keeping all other parameters constant according to the values listed in Table I. Fig. 5(a) and Fig. 5(b) show that the resonant frequencies for both the low and high bands decreases with increasing L_6 and the impedance matching for the upper band, in particular, is also affected. The influence of the monopole end-length parameter L_3 is summarized in Fig. 5(c) and Fig. 5(d). It can be seen that the resonant frequencies for both the lower and upper bands are also seen to decrease for increasing L_3 and the impedance matching for both bands is also affected, particularly for the upper band. The mutual coupling between the spiral and parasitic element accounts for the observed effects as lengthening either element, leads to a decrease in resonant frequencies for both bands. The effects of the varying the shunt inductance length L_S were also investigated but are not plotted here. It was determined that parameter L_S allows a good degree of independent control of the impedance matching for the lower band with a small effect on the resonant frequency for both bands but primarily for the low band. The above parametric simulations show that frequencies f_L and f_H are primarily determined by the total length of the spiral element. The results of Fig. 5 also show that a sufficient degree of independent control is possible using parameters L_3, L_6 and L_S to enable the Lower and Upper frequency bands to be tuned and matched over the frequency range shown. The optimized antenna design parameters are listed in Table I.

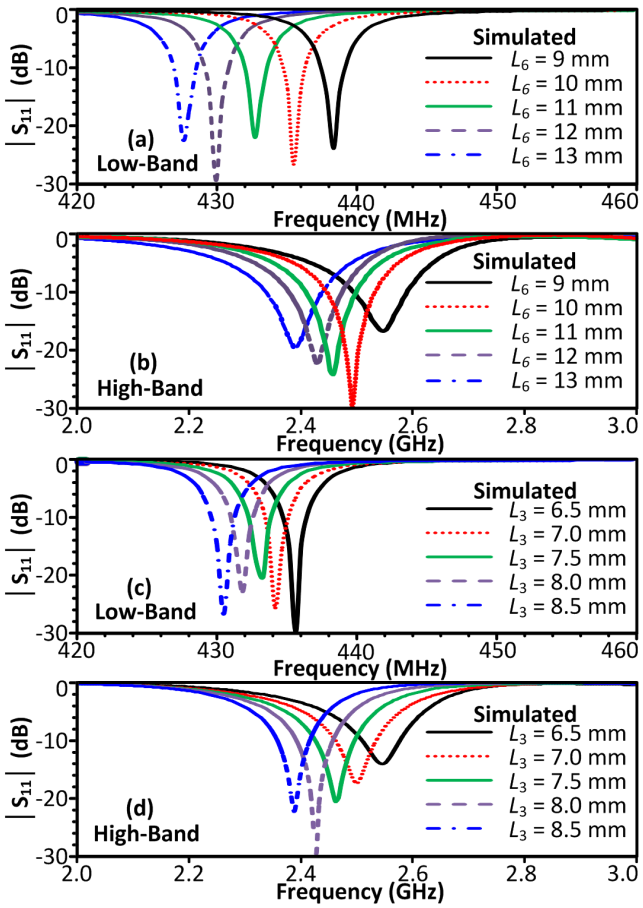

Fig. 5. Simulated $|S_{11}|$ for (a) Varying L_6 Low-band, (b) Varying L_6 High-band, (c) Varying L_3 Low-band, (d) Varying L_3 High-band.

TABLE 1
OPTIMIZED DESIGN PARAMETERS. ALL DIMENSIONS ARE IN MM.

Name	Value	Name	Value	Name	Value	Name	Value
L_1	25.0	L_6	7.56	W_1	1.45	D_4	1.25
L_2	26.0	L_S	6.69	W_2	1.68	D_S	1.88
L_3	11.02	W_G	27.4	D_1	7.30	G	0.50
L_4	8.0	W_F	2.42	D_2	1.00	h	1.53
L_5	0.64	W_S	1.14	D_3	1.00	t_{CU}	0.035

IV. RESULTS AND DISCUSSION

In order to verify the proposed design, a prototype antenna was developed as shown in Fig. 6(a) using a LPKF ProtoMat C60 milling machine. The top and bottom ground interconnections were made using brass pins as shown. The impedance and radiation characteristics of the antenna were then measured in an anechoic chamber using a Vector Network Analyzer. In order to suppress cable current effects, the measurements were performed using a balun and ferrite-beaded cable [2]. The return loss plots of Fig. 6(b) and Fig. 6(c) show the dual-band nature of the antenna and the measured and simulated results show good agreement. The small discrepancies in resonant frequency are most likely attributed to fabrication tolerances for the prototype. The antenna has a measured -10 dB return loss bandwidth of 2 MHz at 433 MHz and 132 MHz at 2.45 GHz that are sufficient to cover the 1.75 MHz and 80 MHz bandwidth requirements.

The measured and simulated radiation patterns for the principal planes are shown in Fig. 7. Overall, the antenna exhibits desirable omni-directional characteristics for both bands and good agreement between measured and simulated results is observed, especially for the *x-z* plane. The differences between the measured and simulated results for the *x-y* and *x-z* planes are attributed to the effects of adding a 90° adapter during these measurements. The addition of the adapter has the effect of moving the axis of measurement away from the phase-centre of the antenna when measuring the *x-y* and *x-z* patterns. In addition, the adapter increases the possibility for coupling between the antenna and the ferrite absorber material and balun, especially for the 2.45 GHz band. Both of the above effects can lead to perturbation of the radiation pattern in the measurement setup and these effects are not modelled in simulation. It can also be observed from

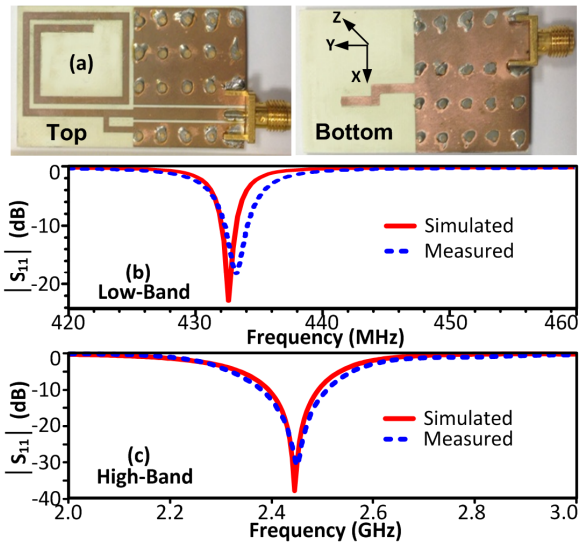

Fig. 6. (a) Photograph of prototype antenna showing top and bottom layers, (b) $|S_{11}|$ for the Low-band, (c) $|S_{11}|$ for the High-Band.

Fig. 7 that the radiation nulls predicted from the current distribution of Fig. 4 are also evident in the measurements.

The peak realized gain was measured as -11.5 dBi at 433 MHz and +0.5 dBi at 2.45 GHz with the maximum gain measured in the *x-z* plane for both frequency bands. The measured gain figures compare well with the simulated values (-10.25 dBi at 433 MHz and 1.45 dBi at 2.45 GHz) and it can be seen that band switching allows adaptive control of antenna gain to suit the link requirements of the application. The

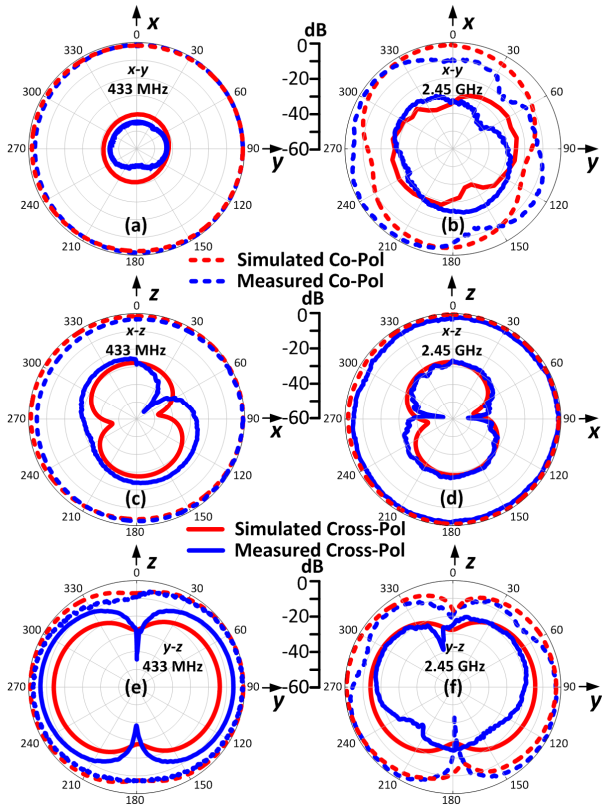

Fig. 7. Measured and simulated radiation patterns: (a) *x-y* plane at 433 MHz, (b) *x-y* plane at 2.45 GHz, (c) *x-z* plane at 433 MHz, (d) *x-z* plane at 2.45 GHz, (e) *y-z* plane at 433 MHz, (f) *y-z* plane at 2.45 GHz.

antenna has a simulated radiation efficiency of approximately 7 % at 433 MHz and 72 % at 2.45 GHz. The relatively low gain and radiation efficiency figures at 433 MHz are expected since the antenna is electrically small [9] but these effects are offset to a large degree by significantly reduced path loss (~15 dB) at 433 MHz when compared to 2.45 GHz.

V. CONCLUSION

In this letter, a compact, single-feed planar antenna that operates in both the 433 MHz and 2.45 GHz ISM bands has been proposed and implemented. Dual-band operation is achieved using a spiral element and a parasitically coupled monopole element. The antenna is realized in a small size of $0.07\lambda \times 0.05\lambda$ at 433 MHz including the groundplane. The antenna is linearly polarized with desirable omni-directional radiation characteristics. The ability of the antenna to cover both the lower and upper extents of the UHF ISM bands together with its small physical size and cost, make it suitable for a wide variety of short-range, wireless applications.

VI. ACKNOWLEDGEMENT

We would like to acknowledge the EC SMArt Systems Co-design project (SMAC) under grant FP7-ICT-2011-7-288827.

VII. REFERENCES

[1] E. Popovici, P. Boyle, S. O'Connell, S. Faul, P. Angove, J. Buckley, B. O'Flynn, J. Barton, and C. O'Mathuna, "The s-Mote: A versatile heterogeneous multi-radio platform for wireless sensor networks applications," in *Circuit Theory and Design (ECCTD), 2011 20th European Conference on*, 2011, pp. 421-424.

[2] L. Loizou, J. Buckley, and B. O'Flynn, "Design and Analysis of a Dual-Band Inverted-F Antenna With Orthogonal Frequency-Controlled Radiation Planes," *Antennas and Propagation, IEEE Transactions on,* vol. 61, pp. 3946-3951, 2013.

[3] C. Yun-Wen and W. Kin-Lu, "Internal Compact Dual-Band Printed Loop Antenna for Mobile Phone Application," *Antennas and Propagation, IEEE Transactions on,* vol. 55, pp. 1457-1462, 2007.

[4] J. Jen-Yea and T. Liang-Chih, "Small planar monopole antenna with a shorted parasitic inverted-L wire for wireless communications in the 2.4-, 5.2-, and 5.8-GHz bands," *Antennas and Propagation, IEEE Transactions on,* vol. 52, pp. 1903-1905, 2004.

[5] M. Fallahpour, M. T. Ghasr, and R. Zoughi, "Miniaturized Reconfigurable Multiband Antenna For Multiradio Wireless Communication," *Antennas and Propagation, IEEE Transactions on,* vol. 62, pp. 6049-6059, 2014.

[6] R. S. Alrawashdeh, Y. Huang, M. Kod, and A. A. B. Sajak, "A Broadband Flexible Implantable Loop Antenna With Complementary Split Ring Resonators," *Antennas and Wireless Propagation Letters, IEEE,* vol. 14, pp. 1322-1325, 2015.

[7] X. Li-Jie, G. Yong-Xin, and W. Wen, "Dual-Band Implantable Antenna With Open-End Slots on Ground," *Antennas and Wireless Propagation Letters, IEEE,* vol. 11, pp. 1564-1567, 2012.

[8] K. Jae Hee, C. Won Woo, and P. Wee Sang, "A Small Dual-Band Inverted-F Antenna With a Twisted Line," *Antennas and Wireless Propagation Letters, IEEE,* vol. 8, pp. 307-310, 2009.

[9] H. A. Wheeler, "Fundamental Limitations of Small Antennas," *Proceedings of the IRE,* vol. 35, pp. 1479-1484, 1947.

[10] J. Buckley, D. Gaetano, K. G. McCarthy, L. Loizou, B. O'Flynn, and C. O'Mathuna, "Compact 433 MHz antenna for wireless smart system applications," *Electronics Letters,* vol. 50, pp. 572-574, 2014.

[11] ANSYS. (2015, Jan). *ANSYS HFSS.* Available: http://www.ansys.com

[12] J. D. Kraus, "Antennas For All Applications," Third ed: McGraw Hill, 2002, pp. 181-183.